Skyrmion-induced bound state in a two-dimensional superconductor

Sho Nakosai[1,2], Sergey S. Pershoguba[1], and Alexander V. Balatsky[1,3]
[1] *Nordita, Center for Quantum Materials, KTH Royal Institute of Technology, and Stockholm University, Roslagstullsbacken 23, S-106 91 Stockholm, Sweden*
[2] *Department of Applied Physics, University of Tokyo, Tokyo 113-8656, Japan and*
[3] *Institute for Materials Science, Los Alamos National Laboratory, Los Alamos, NM 87545, USA*
(Dated: September 24, 2015)

We consider a superconductor proximity coupled to a 2D ferromagnetic film with a topological configuration of the ferromagnetic vector, i.e. the skyrmion. Using the T-matrix calculations as well as well numerical modeling we calculate the spin-polarized local density of states (SP-LDOS) in the vicinity of the skyrmion. We identify a skyrmion bound state (SBS), calculate its energy and a spectral width. The SBS resonance has a long-ranged spatial power-law decay. This implies that superconductivity could facilitate a long-range interaction between distinct skyrmions on the surface of the ferromagnetic film.

PACS numbers:

Introduction. Skyrmions, particle-like topological configurations of a continuous field, were originally proposed in the context of high-energy physics. Nevertheless, it was suggested theoretically [1, 2] and recently observed experimentally [3–7] that skyrmions exist in chiral ferromagnets in the presence of Dzyaloshinkii-Moriya interaction, which is allowed when inversion symmetry is broken. The skyrmions in ferromagnetic films hold great promise in spintronic applications. Due to nontrivial topological properties of skyrmions, they manifest anomalous response to temperature gradients [8] and electric field [9]. Recently, Hamburg group demonstrated controllable writing and deleting of single skyrmions on the surface of PdFe bilayer [10–12].Coupling of magnetic films with skyrmions to novel materials holds a new promising avenue. Coupling of skyrmion to a topological insulatorswas considered in Ref. [13]. These developments show that skyrmions hold great promise in applications such as spintronics, memory devices, etc [14].

In parallel, there has been a considerable amount of interest recently in ferromagnet-superconductor heterostructures aimed at engineering topological superconductors [15]. Discovery of such topological superconductiviy entails existence of Majorana edge modes in these systems, which would pave the way to realizing topological quantum computing [16]. So, motivated by the immense interest in ferromagnetic skyrmions and the ferromagnet-superconductor heterostructures, we bridge the connection between the two fields in the current paper and study a superconductor priximity-coupled to a thin film with a skyrmionic configuration of a ferromagnetic vector as illustrated in Fig. 1. Few works have considered skyrmions in the context of superconductivity. In Ref. [17], authors discuss the skyrmions in momentum space of the topological superconductors. Reference [18] studied the skyrmion-defects in the multiband superfluids and superconductors. A closely related work [19] discussed a possibility of realizing a topological superconductor using a skyrmionic lattice. The Josephson current through a magnetic skyrmion structure was considered

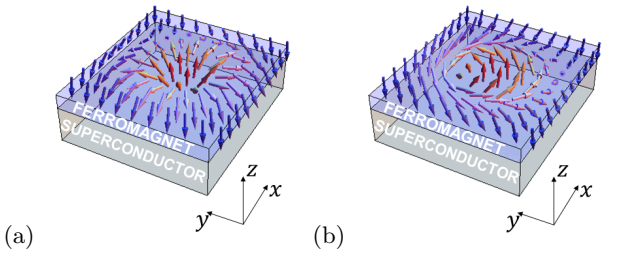

FIG. 1. (Color online.) Ferrormagnetic film deposited on top of a superconductor. The ferromagnetic vector has skyrmion configuration. (a) Bloch-type skyrmion. (b) Neel-type skyrmion.

in Ref. [20]. However, none of the papers considered the conceptually simplest case of interaction between a single skyrmion a superconductor that is discussed in the current work.

First and foremost, superconductivity could be useful in stabilizing the skyrmionic phase. The superconductivity, e.g. in non-centrosymmetric materials, could induce effective Dzyaloshinskii-Moriya interaction between the ferromagagnetic spins and, thus, stabilize the skyrmionic phase. A number of recent theoretical claims of a strong interaction between the magnetic impurities via tha superconducting host [21, 22] support that proposal. Using similar arguments, the superconductivity could mediate effective interaction between the skyrmions and, thus, affect their dynamics.

In the current paper we consider a ferromagnetic film with a skyrmion proximity coupled to a superconductor as shown in Fig. 1. We study a state induced by a skyrmion in a superconductor. In a close analogy with the Yu-Shiba-Rusinov [23–25] states, we find a skyrmion bound state (SBS), a state localized around a skyrmion, using an analytical T-matrix calculation. The energy of SBS typically lies in between the superconducting bands corresponding to the delocolized states of the opposite spin-polarization. Since skyrmion is a complex object

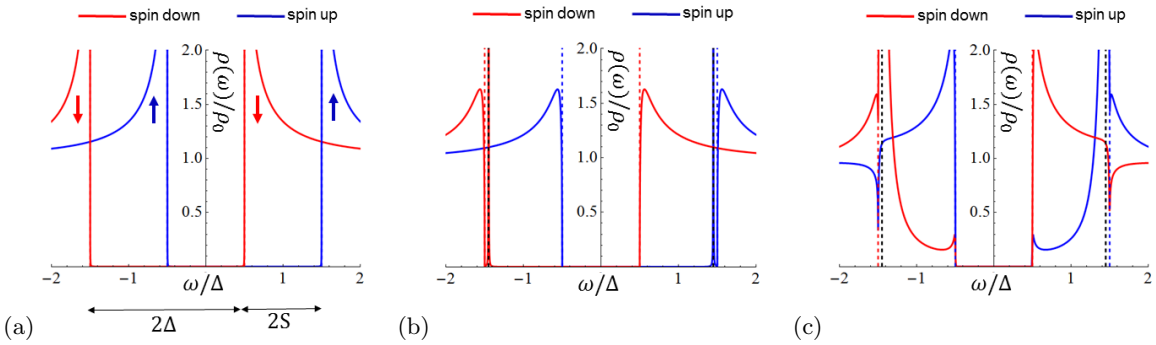

FIG. 2. (Color online) Spin-polarized local density of states (a) away from the skyrmion and (b,c) at the core of the skyrmion. Panel (b) corresponds to the usual T-matrix that takes into account only out-of-plane. Panel (c) corresponds to the T-matrix that takes into account in-plane spin. Comparing (b) and (c) notice that a thin YSR state in (b) becomes a thick resonance in (c). The parameters of plots are $2S = \Delta = 0.25E_F$ and $R = 1/p_F = \xi/8$. Blue and red dashed lines indicate the positions of the shifted spin-up and spin-down bands, respectively. The black dashed line indicates the position of the YSR pole, given by Eq. .

with spins in all directions the spin-up and spin-down sectors of the Hamiltonian are coupled, and SBS is a resonance with a finite spectral width. We calculate a spin-polarized local density of states (SP-LDOS) in the vicinity of skyrmions that could be measured using spin-polarized scanning tuneling micropscopy (SP-STM) [10–12]. In contrast, with the conventional YSR states, the SBS state is a long-ranged state with a powerlaw decay. Therefore, in the presence of a second skyrmion, the SBS states will interact and give a strong [21] long-ranged "Casimir" interaction [26] between the skyrmions.

Skyrmions in ferromagnetic films. Let the three-dimensional vector $S(\boldsymbol{r}) = (S_x, S_y, S_z)$ describe the configuration of the ferromagnetic vector in a two-dimensional ferromagnetic film $\boldsymbol{r} = (x, y)$. The configurations of the field $S(\boldsymbol{r})$ shown in Fig. 1(a) and (b) are referred to as skyrmions. The skyrmion configuration of the field is characterized by the topological charge

$$Q = \frac{1}{4\pi}\int d^2r\, \hat{\boldsymbol{S}}\cdot(\nabla_x\hat{\boldsymbol{S}}\times\nabla_y\hat{\boldsymbol{S}}), \quad \hat{\boldsymbol{S}} = \frac{\boldsymbol{S}}{S}, \tag{1}$$

which cannot be altered by the continuous transfomation of the field. We also characterize the skyrmion fields by the zeroth and first moments

$$S_i^{(0)} = \int d^2r\, \left[S_i(\boldsymbol{r}) - S_i(\infty)\right],\ i \in \{x, y, z\}, \tag{2}$$

$$S_{ij}^{(1)} = \int d^2r\, \left[S_i(\boldsymbol{r}) - S_i(\infty)\right] r_j,\ j \in \{x, y\}. \tag{3}$$

The zeroth moment $\boldsymbol{S}^{(0)} = S_{\rm e}\hat{\boldsymbol{z}}$ characterizes the effective out-of-plane magnetic moment of the skyrmion and is equal for the two skyrmions shown in Fig. 1(a) and (b). Whereas, the first-order moment $S_{ij}^{(1)}$ characterizes the in-plane pattern of the ferromagnetic vector $\boldsymbol{S}(\boldsymbol{r})$. Note that for the cylindrically symmetric field $S(\boldsymbol{r})$, the first order moment defined in Eq. (3) can be expanded in the symmetric and antisymmetric parts

$$S_{ij}^{(1)} = S_{\rm m}\,\delta_{ij} + S_{\rm a}\,\epsilon_{ijz} \tag{4}$$

The skyrmions shown in Fig. 1(a) and (b) have monopole $S_{\rm m}$ and anapole $S_{\rm a}$ moments correspondingly, hence the name of the skyrmions. However the two types of the skyrmions have the same topological charge (1) and can be continuosly deformed into each other.

Model The model is given by the following 4-by-4 Bogolyubov-de Gennes (BdG) Hamiltonian

$$H = \xi(\boldsymbol{p})\tau_z + \Delta\tau_x - \boldsymbol{S}(\boldsymbol{r})\cdot\boldsymbol{\sigma}, \tag{5}$$

$$\xi(\boldsymbol{p}) = \frac{p^2}{2m} - \mu, \quad \boldsymbol{p} = -i(\nabla_x, \nabla_y), \tag{6}$$

which describes the proximity coupling of the ferromagnetic vector $S(\boldsymbol{r})$ to the itinerant electrons of a two-dimensional (2D) superconductor with the superconducting gap Δ. The Pauli matrices $\boldsymbol{\tau}$ and $\boldsymbol{\sigma}$ act, respectively, in the particle-hole and spin subspaces of the four-component spinor $\Psi = (\psi_\uparrow, \psi_\downarrow, \psi_\downarrow^\dagger, -\psi_\uparrow^\dagger)^T$. For simplicity, we assume that the magnitude of the superconductor-ferromagnet coupling is constant and only the direction $\boldsymbol{S}(\boldsymbol{r})$ varies, i.e. we set $\boldsymbol{S}(\boldsymbol{r}) = S\,\boldsymbol{n}(\boldsymbol{r})$, where $\boldsymbol{n}$ is a unit vector. In order to proceed further let compare the typical lengthscales. The radius of skyrmions R found in experiments [6, 10–12, 27–29] does not typically exceed 5 nm, whereas the superconducting coherence length ξ_{sc} varies largely from a micron to a few nanometers as in, e.g., curprates. For the analysis below, we assume the superconducting coherence length much larger $\xi_{sc} \gg R$, and briefly comment about the opposite limit in the Supplemental Material (Shall we discuss this? Local gauge transform and introduce effective spin-orbit, etc.). In the chosen limit the superconductivity cannot "resolve" the fine details of the field $\boldsymbol{S}(\boldsymbol{r})$ and only "sees" as a skyrmion as local magnetic defect. Therefore we shall apply a Yu-Shiba-Rusinov [23–25, 30] treatment the skyrmion as a local impurity.

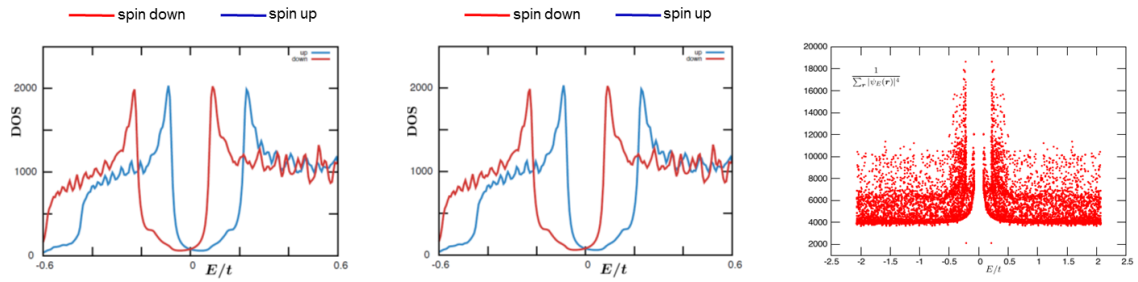

(a) (b) (c)

FIG. 3. (Color online) Numerical modeling of a skyrmion: (a) LDOS away from the skyrmion (PLEASE SUBSTITUTE WITH THE CORRECT FIGURE), (b) LDOS at the skyrmion core, (c) inverse participation ratio (IPR).

T-matrix analysis It is convenient to split the Hamiltonian (5) $H = h(\boldsymbol{p}) + V(\boldsymbol{r})$ into the spatially uniform part $h(\boldsymbol{p})$ and a local perturbation $V(\boldsymbol{r})$ describing the skyrmion

$$h(\boldsymbol{p}) = \xi(\boldsymbol{p})\tau_z + \Delta\tau_x - \boldsymbol{S}(\infty)\cdot\boldsymbol{\sigma}, \quad \boldsymbol{S}(\infty) = -S\,\hat{\boldsymbol{z}} \quad (7)$$

$$V(\boldsymbol{r}) = -\left[\boldsymbol{S}(\boldsymbol{r}) - \boldsymbol{S}(\infty)\right]\cdot\boldsymbol{\sigma} \quad (8)$$

For the skyrmions shown in Figs. 1(a) and (b), the ferromagnetic vector is $S(\infty) = -S\,\hat{\boldsymbol{z}}$ far from skyrmion, and is parallel to $\boldsymbol{S}(0) = S\hat{\boldsymbol{z}}$ at the skyrmion core. The Hamiltonian $h(\boldsymbol{p})$ describes a superconductor proximity coupled to a ferromagnet with constant magnetization, i.e. in the absence of the skyrmion. The ferromagnetic term $S\sigma_z$ breaks two-fold Kramers degeneracy of the bands and the spectrum contains four coherence peaks with energies $\pm\Delta \pm S$ as shown in Fig. (2)(a). The bands corresponding to opposite spin are decoupled. The spectrum maintains a gap as long as the Zeeman coupling is less than the superconducting gap, i.e. $S < \Delta$. Such spectrum should be possible to detect by the spin-polarized tunneling spectroscopy methods[cite relevant papers]. In the presence of the skyrmion, the term (8) should be taken into account. As pointed out above, for small skyrmion size $\xi_{sc} \gg R$, the skyrmion field can be approximated as a local magnetic impurity with $V(\boldsymbol{r}) = S_{\rm e}\,\sigma_z\delta^2(\boldsymbol{r})$[1]. Such a local perturbation can be treated exactly by calculating the T-matrix

$$T(\omega) = \frac{-S_{\rm e}\sigma_z}{1 + S_{\rm e}\sigma_z g_0(\omega)} \quad (9)$$

taken into account in T-matrix calculation, which gives the following SP-LDOS at the skyrmion core

$$\rho_s(\omega) = \quad (10)$$
$$-\frac{1}{\pi}\,\mathrm{Im}\,\mathrm{Tr}\left\{\frac{1+\tau_z}{2}\,\frac{1+\sigma_s}{2}\left[g_0(\omega) + g_0(\omega)T(\omega)g_0(\omega)\right]\right\},$$

[1] Using Eqs. (2) and (3), the moments can be expressed via the original parameters of the model as $S_{\rm e} = c_1 SR^2$ and $S_{\rm m} = c_2 SR^3$, where S is ferromagnetic coupling and R - the skyrmion radius. The coefficients $c_1 \approx 5.18$ and $c_2 \approx 6.53$ are calculated in the Supplementary Material for a specific model.

where energy has infinitesimally small imaginary part in the right side of the equation, i.e. $\omega \to \omega + i\delta$, and $s = x, y, z$ denotes the spin quantization axis. In Eqs. (9) and (10), the $g_0(\omega)$ is the on-site matrix element of the Green's function $g(\omega, \boldsymbol{p}) = [\omega - h(\boldsymbol{p})]^{-1}$

$$g_0(\omega) = -\pi\rho\sum_{\lambda=\pm1}\frac{1+\lambda\sigma_z}{2}\,\frac{\omega - \lambda S + \Delta\tau_x}{\sqrt{\Delta^2 - (\omega - \lambda S)^2}}, \quad (11)$$

where $\rho = m/2\pi$ is the density of states. We plot LDOS (10) in Fig. 2(b). We observe that the skyrmion-YSR (SYSR) states split from the bulk bands. The energy of the states is given by the poles of the T-matrix, i.e. satisfy the equation $1 + S_{\rm e}\sigma_z g_0(\omega) = 0$, which gives

$$E^{\pm}_{\rm SYSR} = \pm\left[S + \Delta\frac{1 - (\pi\rho S_{\rm e})^2}{1 + (\pi\rho S_{\rm e})^2}\right]. \quad (12)$$

The SYSR states maintain the spin polarization of the bands they split off: the positive (negative) SYSR state "up" ("down") spin-polarized. For small skyrmions $R \sim 1/p_F$, the effective magnetic moment of a skyrmion $S_{\rm e}$ is small, and, so, the SYSR states are close to the outter coherence peaks $\pm(\Delta + S)$ as seen in Fig. 2(b). Therefore the SYSR states lie inside continuum of states with the opposite spin. In the absence of coupling between the spin-"up" and "down" sectors of the Hamiltonian, the SYSR states do not mix with the background delocalized states and maintain zero spectral width. In this respect, they do not differ much from the conventional YSR states.

In such a way, we have shown that the skyrmion can be treated as a point impurity and induces a YSR-like state in the spectrum. Let us now expand the model by taking into account that the in-plane spins, which are unavoiably present around the skyrmion, can couple the up and down sectors of the Hamiltonian. As discussed above, the in-plane spins are characterized by the first moment tensor Eq. (3). In the case of the hedgehog skyrmion, the tensor only contains the diagonal component corresponding to the monopole moment $S_{\rm m}$. Therefore we modify the local perturbation describing the skyrmion as $V(\boldsymbol{r}) = S_{\rm e}\,\sigma_z\delta^2(\boldsymbol{r}) - S_{\rm m}\,\boldsymbol{\sigma}\cdot\boldsymbol{\nabla}\delta^2(\boldsymbol{r})$.

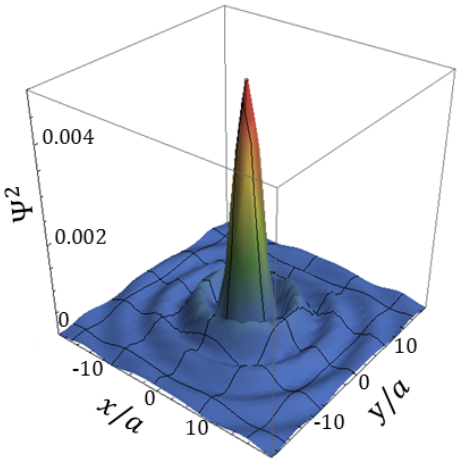

FIG. 4. (Color online) Numerical wavefunction corresponding to the sYSR state. The wave function has pronounced oscillations with a period of approximately the superconducting coherence length. [parameters for which the figures are plotted]

We repeat the T-matrix calculation for this perturbation in the Supplementary Material and obtain

$$T(\omega) = \frac{-S_{\rm e}\sigma_z + S_{\rm m}^2 p_F^2 \bar{g}_0(\omega)}{1 + S_{\rm e}\sigma_z g_0(\omega) - S_{\rm m}^2 p_F^2\, \bar{g}_0(\omega)\, g_0(\omega)}, \qquad (13)$$

where for brevity $\bar{g}_0(\omega) = \frac{1}{2}\sum_{j=x,y} \sigma_j g_0(\omega)\sigma_j$ is the Green's function obtained from Eq. (11) by substitution $\sigma_z \to -\sigma_z$. We compare Eqs. (9) and (13) and observe that the latter contains renormalized numerator and the denominator due to S_m. We substitue the T-matrix (13) in Eq. (10) and plot LDOS in Fig. 2(c). We observe the LDOS around the SYSR state has significantly widened. In order to explain this, let us consider poles of the T-matrix (13) given by $1 + S_{\rm e}\sigma_z g_0(\omega) - S_{\rm m}^2 p_F^2\, \bar{g}_0(\omega)\, g_0(\omega) = 0$. The real part of this equation still gives the SYSR state given by Eq. (12). However, since $\bar{g}_0(\omega)$, which is the Green's function for a flipped spin, is imaginary at the SYSR energy, the term $S_{\rm m}^2 p_F^2\, \bar{g}_0(\omega)\, g_0(\omega)$ becomes imaginary and determines a finite spectral width of SYSR resonance. The LDOS also manifests an upshoot This explains the apparent widening of the spectrum around the SYSR state. The LDOS even contains an upshoot around the inner coherence peaks $\pm(\Delta - S)$.

Numerical analysis. Briefly introduce the model and the results. Compare to analytics. Discuss what is IPR and that it shows only a single quasi localized state. Show IPR for a smaller window of energies, e.g. $-2\Delta < \omega < 2\Delta$. Does the IPR figure correspond to the LDOS figures, or is it plotted for different parameters.

Long-range wave function Now let us show that the wave function corresponding to the SYSR state has a long-range power-law behavior. In general (as also discusssed in appendix), the wave function of an impurity induced state is described by the wave function

$$\Psi(\boldsymbol{r}) \sim \frac{e^{ip_F r} e^{-r\sqrt{\Delta^2 - \omega_\lambda^2}/v_F}}{\sqrt{r}}, \qquad (14)$$

where for brevity λ denotes the eigenvalues of σ_z operator and $\omega_\lambda = \omega - \lambda S$. The former exponential term in Eq. (14) describes the fast Friedel oscillations, whereas latter term - behavior at a scale of superconducting coherence length. For clarity, let us discuss the positive SYSR state, i.e. $\omega = \omega^+_{\rm SYSR}$. It lies inside the superconducting for the spin-up subsystem, i.e. $|\omega_+| < \Delta$, and therefore the latter exponential term in Eq. (14) describes the exponentially dacaying behavior. However, the SYSR state also couples to the background spin-down subsystem, for which it is supragap state, i.e. $|\omega_-|$. Therefore, the square root in the Eq. (14) becomes imaginary $\sqrt{\Delta^2 - \omega_-^2} = -i\sqrt{\omega_-^2 - \Delta^2}$, which describes oscillating rather than decaying behavior at a scale ξ_{sc}. Colloquially speaking, the exponentiall localized YSR state couples to the delocalized states and becomes long-range. This is also supported by the numerical wavefunction which manifest periodic oscillations at a scale of ξ_{sc} as shownn in Fig. 4. [Discuss that IPR should see the power law decay (i.e. change of IPR with system size)]

Conclusion There are two effects: local scattering and Zeeman field hence the DOS will be split etc. Draw similarities and differences with single imp. In parallel with skyrmion discovery the local imaging using magnetic probes like MFM and SP-STM allowed one to image the matter at atomic resolution while also resolving spin content of electron carriers in the substrate. Here we prove the existence of the new type of localized excitation on the skyrmion core we call Sc-YSR state (alternative is skyrmion bound state (sbs)). Show the main results upfront in the introduction. Both LDOS and SP-LDOS.

We thank A. Saxena, Y. Kedem, for useful discussions. This work was supported by the European Research Council (ERC) DM-321031 and the US DOE BES E304 (S.S.P. and A.V.B.).

[1] A. N. Bogdanov and D. A. Yablonskii, "Thermodynamically stable "vortices" in magnetically ordered crystals. The mixed state of magnets." Sov. Phys. JETP **68**, 101 (1989).

[2] U K Rössler, A N Bogdanov, and C Pfleiderer, "Spontaneous skyrmion ground states in magnetic metals." Nature **442**, 797 (2006).

[3] S Mühlbauer, B Binz, F Jonietz, C Pfleiderer, A Rosch, A Neubauer, R Georgii, and P Böni, "Skyrmion lattice in a chiral magnet." Science **323**, 915 (2009).

[4] W. Münzer, A. Neubauer, T. Adams, S. Mühlbauer, C. Franz, F. Jonietz, R. Georgii, P. Böni, B. Pedersen, M. Schmidt, A. Rosch, and C. Pfleiderer, "Skyrmion lattice in the doped semiconductor $Fe_{1-x}Co_xSi$," Phys. Rev. B **81**, 041203 (2010).

[5] X. Z. Yu, N. Kanazawa, Y. Onose, K. Kimoto, W. Z. Zhang, S. Ishiwata, Y. Matsui, and Y. Tokura, "Near room-temperature formation of a skyrmion crystal in thin-films of the helimagnet FeGe," Nat. Mater. **10**, 106 (2011).

[6] S. Heinze, K. von Bergmann, M. Menzel, J. Brede, A. Kubetzka, R. Wiesendanger, G. Bihlmayer, and S. Blügel, "Spontaneous atomic-scale magnetic skyrmion lattice in two dimensions," Nat. Phys. **7**, 713 (2011).

[7] S. Seki, X. Z. Yu, S. Ishiwata, and Y. Tokura, "Observation of Skyrmions in a Multiferroic Material," Science **336**, 198 (2012).

[8] F. Jonietz, S. Mhlbauer, C. Pfleiderer, A. Neubauer, W. Mnzer, A. Bauer, T. Adams, R. Georgii, P. Bni, R. A. Duine, K. Everschor, M. Garst, and A. Rosch, "Spin Transfer Torques in MnSi at Ultralow Current Densities," Science **330**, 1648 (2010).

[9] A. Neubauer, C. Pfleiderer, B. Binz, A. Rosch, R. Ritz, P. G. Niklowitz, and P. Böni, "Topological Hall Effect in the A Phase of MnSi," Phys. Rev. Lett. **102**, 186602 (2009).

[10] N. Romming, C. Hanneken, M. Menzel, J. E. Bickel, B. Wolter, K. von Bergmann, A. Kubetzka, and R. Wiesendanger, "Writing and Deleting Single Magnetic Skyrmions," Science **341**, 636 (2013).

[11] K. von Bergmann, A. Kubetzka, O. Pietzsch, and R. Wiesendanger, "Interface-induced chiral domain walls, spin spirals and skyrmions revealed by spin-polarized scanning tunneling microscopy," J. Phys.: Condens. Matter **26**, 394002 (2014).

[12] N. Romming, A. Kubetzka, C. Hanneken, K. von Bergmann, and R. Wiesendanger, "Field-Dependent Size and Shape of Single Magnetic Skyrmions," Phys. Rev. Lett. **114**, 177203 (2015).

[13] Hilary M. Hurst, Dmitry K. Efimkin, Jiadong Zang, and Victor Galitski, "Charged skyrmions on the surface of a topological insulator," Phys. Rev. B **91**, 060401 (2015).

[14] N. Nagaosa and Y. Tokura, "Topological properties and dynamics of magnetic skyrmions," Nat. Nanotechnol. **8**, 899 (2013).

[15] Jason Alicea, "New directions in the pursuit of Majorana fermions in solid state systems." Rep. Prog. Phys. **75**, 076501 (2012).

[16] Chetan Nayak, Steven H. Simon, Ady Stern, Michael Freedman, and Sankar Das Sarma, "Non-abelian anyons and topological quantum computation," Rev. Mod. Phys. **80**, 1083–1159 (2008).

[17] Kristofer Björnson and Annica M. Black-Schaffer, "Skyrmion spin texture in ferromagnetic semiconductor-superconductor heterostructures," Phys. Rev. B **89**, 134518 (2014).

[18] Julien Garaud, Johan Carlström, and Egor Babaev, "Topological solitons in three-band superconductors with broken time reversal symmetry," Phys. Rev. Lett. **107**, 197001 (2011).

[19] S. Nakosai, Y. Tanaka, and N. Nagaosa, "Two-dimensional p-wave superconducting states with magnetic moments on a conventional s-wave superconductor," Phys. Rev. B **88**, 180503 (2013).

[20] Takehito Yokoyama and Jacob Linder, "Josephson effect through magnetic skyrmions," Phys. Rev. B **92**, 060503 (2015).

[21] N. Y. Yao, L. I. Glazman, E. A. Demler, M. D. Lukin, and J. D. Sau, "Enhanced Antiferromagnetic Exchange between Magnetic Impurities in a Superconducting Host," Phys. Rev. Lett. **113**, 087202 (2014).

[22] G. C. Ménard, S. Guissart, C. Brun, S. Pons, V. S. Stolyarov, F. Debontridder, M. V. Leclerc, E. Janod, L. Cario, D. Roditchev, P. Simon, and T. Cren, "Long range coherent magnetic bound states in superconductors," arXiv:1506.06666.

[23] L. Yu, "Bound state in superconductors with paramagnetic impurities," Acta Phys. Sin. **21**, 75 (1965).

[24] H. Shiba, "Classical Spins in Superconductors," Prog. Theor. Phys. **40**, 435 (1968).

[25] A. I. Rusinov, "Superconductivity near a paramagnetic impurity," JETP Lett. **9**, 85 (1969).

[26] Andrei V. Shytov, Dmitry A. Abanin, and Leonid S. Levitov, "Long-range interaction between adatoms in graphene," Phys. Rev. Lett. **103**, 016806 (2009).

[27] J. Brede, N. Atodiresei, V. Caciuc, M. Bazarnik, A. Al-Zubi, S. Blügel, and R. Wiesendanger, "Long-range magnetic coupling between nanoscale organicmetal hybrids mediated by a nanoskyrmion lattice," Nat. Nanotechnol. **9**, 1018 (2014).

[28] A. Sonntag, J. Hermenau, S. Krause, and R. Wiesendanger, "Thermal Stability of an Interface-Stabilized Skyrmion Lattice," Phys. Rev. Lett. **113**, 077202 (2014).

[29] K. von Bergmann, M. Menzel, A. Kubetzka, and R. Wiesendanger, "Influence of the Local Atom Configuration on a Hexagonal Skyrmion Lattice," Nano Lett. **15**, 3280 (2015).

[30] A. V. Balatsky, I. Vekhter, and J.-X. Zhu, "Impurity-induced states in conventional and unconventional superconductors," Rev. Mod. Phys. **78**, 373 (2006).

[31] F. Pientka, L. I. Glazman, and F. von Oppen, "Topological superconducting phase in helical Shiba chains," Phys. Rev. B **88**, 155420 (2013).

Appendix A: T-matrix analysis

In this section, we give an analytic treatment of the skyrmion-induced bound states using the T-matrix approximation. Starting from the Hamiltonian (5) in the second-quantized form, we write the Bogolyubov-de Gennes (BdG) Hamiltonian as

$$H_{\rm BdG} = h(\boldsymbol{p}) + V(\boldsymbol{r}), \quad \text{where} \tag{A1}$$

$$H(\boldsymbol{p}) = \xi(\boldsymbol{p})\tau_z + \Delta\tau_x - \boldsymbol{S}(\infty)\cdot\boldsymbol{\sigma}, \quad \boldsymbol{S}(\infty) = -S\,\hat{\boldsymbol{z}},$$

$$V(\boldsymbol{r}) = -\left[\boldsymbol{S}(\boldsymbol{r}) - \boldsymbol{S}(\infty)\right]\cdot\boldsymbol{\sigma} \tag{A2}$$

The momentum-dependent part $H(\boldsymbol{p})$ describes a superconductor coupled to a spatially uniform ferromagnetic vector $\boldsymbol{S}(\infty)$, whereas the position-dependent piece $V(\boldsymbol{r})$ describes the local perturbation due to the skyrmion. Although the specific model is not significant, we assume the following model for the skyrmion centered at the ori-

gin $r = 0$

$$\boldsymbol{S}(\boldsymbol{r}) = S\left[\cos\phi(\boldsymbol{r})\sin\theta(\boldsymbol{r}),\, \sin\phi(\boldsymbol{r})\sin\theta(\boldsymbol{r}),\, \cos\theta(\boldsymbol{r})\right],$$
$$\phi(\boldsymbol{r}) = \arctan(x/y), \quad \theta(\boldsymbol{r}) = \pi\left[1 - \exp\left(-\frac{r^2}{R^2}\right)\right], \tag{A3}$$

where $\phi(\boldsymbol{r})$ and $\theta(\boldsymbol{r})$ denote the polar and azimuthal angle of the vector $\boldsymbol{S}(\boldsymbol{r})$, and R controls the skyrmion size. The superconducting coherence length is usually greater than a typical skyrmion size $R \sim 5\,\mathrm{nm}$ [6, 10–12, 27–29], i.e. $\xi_{\mathrm{sc}} \gg R$. Therefore, the superconductivity does not "resolve" the fine details of the skyrmionic configuration of the field $\boldsymbol{S}(\boldsymbol{r})$, but rather "sees" its long-wavelength characteristics such as the moments described by Eqs. (2) and (3). Motivated by this logic, we substitute the original skyrmionic field $\boldsymbol{S}(\boldsymbol{r})$ by its local version

$$\boldsymbol{S}(\boldsymbol{r}) - \boldsymbol{S}(\infty) = \left[S_{\mathrm{e}}\,\hat{\boldsymbol{z}} - S_{\mathrm{m}}\,\boldsymbol{\nabla}\right]\delta^2(\boldsymbol{r}). \tag{A4}$$

Here, in order to relate the moments to the original parameters of the model we subtitute Eq. (A3) in Eqs. (2) and (3) and find

$$S_{\mathrm{e}} = SR^2\pi\left[-\mathrm{Ci}(\pi) + \gamma + \log(\pi)\right] \approx 5.18\,SR^2, \tag{A5}$$
$$S_{\mathrm{m}} = SR^3\int_0^\infty 2\pi t^2 \sin\left(\pi e^{-t^2}\right)\,dt \approx 6.53\,SR^3. \tag{A6}$$

Equation (A4) is convenient for the T-matrix calculation, which we now proceed to. We take into account (A4) and calculate the Fourier transform of Eq. (A2)

$$V(\boldsymbol{p}) = -S_{\mathrm{e}}\,\sigma_z + i\,S_{\mathrm{m}}\,\boldsymbol{\sigma}\cdot\boldsymbol{p}, \tag{A7}$$

using which we write an intergal equation for the T-matrix

$$T\left(\boldsymbol{p}^1, \boldsymbol{p}^2\right) = V\left(\boldsymbol{p}^1 - \boldsymbol{p}^2\right) + \int \frac{d^2p'}{(2\pi)^2}\,V\left(\boldsymbol{p}^1 - \boldsymbol{p}'\right)g(\omega, \boldsymbol{p}')T\left(\boldsymbol{p}', \boldsymbol{p}^2\right). \tag{A8}$$

Here, the bare Green's function of the superconductor is defined as

$$g(\omega, \boldsymbol{p}) = \frac{1}{\omega - h(\boldsymbol{p})} = \frac{1}{\omega - \xi(\boldsymbol{p})\tau_z - \Delta\tau_x - S\sigma_z}. \tag{A9}$$

Since in the case of the superconductivity we are interested in the scatterings close to the Fermi surface, we use $\boldsymbol{p}^1 = p_F\,\boldsymbol{n}^1$ and $\boldsymbol{p}^2 = p_F\,\boldsymbol{n}^2$, where the in-plane unit vectors $\boldsymbol{n}^1$ and $\boldsymbol{n}^2$ determine the direction of scattering on the Fermi surface. Then, we seek the T-matrix in the following form

$$T\left(\boldsymbol{n}^1, \boldsymbol{n}^2\right) = A + B_i n_i^1 + C_i n_j^2 + D_{ij} n_i^1 n_j^2, \tag{A10}$$

where A, B_i, C_i and D_{ij} are the matrices in the four-components space $\sigma \otimes \tau$. We substitute ansatz (A10) in the integral Eq. (A8) and find the T-matrix

$$T\left(\boldsymbol{n}^1, \boldsymbol{n}^2\right) = \frac{-S_{\mathrm{e}}\sigma_z + S_{\mathrm{m}}^2 p_F^2\,\bar{g}_0(\omega) + i\,S_{\mathrm{m}}\,p_F\,\boldsymbol{\sigma}\cdot(\boldsymbol{n}^2 - \boldsymbol{n}^1) + S_{\mathrm{m}}^2\,p_F^2\,\bar{g}_0(\omega)\,\left(\boldsymbol{\sigma}\cdot\boldsymbol{n}^2\right)\,\left(\boldsymbol{\sigma}\cdot\boldsymbol{n}^1\right)}{1 + S_{\mathrm{e}}\sigma_z g_{00} - S_{\mathrm{m}}^2 p_F^2\,\bar{g}_0(\omega)\,g_0(\omega)}, \tag{A11}$$

where the Green's function on-site matrix element in the real space is denoted as

$$g_0(\omega) = \int \frac{d^2p}{(2\pi)^2}\,g(\omega, \boldsymbol{p}) = -\pi\rho\sum_{\lambda=\pm1}\frac{1+\lambda\sigma_z}{2}\,\frac{\omega - \lambda S + \Delta\tau_x}{\sqrt{\Delta^2 - (\omega - \lambda S)^2}}, \tag{A12}$$
$$\bar{g}_0(\omega) = \frac{1}{2}\sum_{j=x,y}\sigma_j\,g_0(\omega)\,\sigma_j. \tag{A13}$$

For brevity, $\bar{g}_0$ denotes the Green's function obtained from g_{00} by replacing $\sigma_z \to -\sigma_z$ according to Eq. (A13). The density of states per spin is denoted as $\rho = m/2\pi$. So, in the presence of the skyrmion, the Green's function becomes

$$G(\omega, \boldsymbol{p}^1, \boldsymbol{p}^2) = g(\omega, \boldsymbol{p}^1)\,(2\pi)^2\delta(\boldsymbol{p}^1 - \boldsymbol{p}^2) + g(\omega, \boldsymbol{p}^1)T(\boldsymbol{p}^1, \boldsymbol{p}^2)g(\omega, \boldsymbol{p}^2), \tag{A14}$$

using which the spin-polarized local density of states (LDOS) can be expressed

$$\rho_s(\omega, \boldsymbol{r}) = -\frac{1}{\pi}\,\mathrm{Im}\lim_{\omega\to\omega+i\delta}\mathrm{Tr}\left[\frac{1+\tau_z}{2}\,\frac{1+\sigma_s}{2}\int\frac{d^2p^1\,d^2p^2}{(2\pi)^4}e^{i(\boldsymbol{p}^1-\boldsymbol{p}^2)\boldsymbol{r}}G(\omega, \boldsymbol{p}^1, \boldsymbol{p}^2)\right] \tag{A15}$$

where $s = x, y, z$ denotes the spin quantization axis. It can be easily evaluated for instance at the skyrmion core, i.e. at $\boldsymbol{r} = 0$,

$$\rho_s(\omega, 0) = -\frac{1}{\pi}\,\mathrm{Im}\lim_{\omega\to\omega+i\delta}\mathrm{Tr}\left\{\frac{1+\tau_z}{2}\,\frac{1+\sigma_s}{2}\left[g_0(\omega) + g_0(\omega)\frac{-S_{\mathrm{e}}\sigma_z + S_{\mathrm{m}}^2 p_F^2\bar{g}_0(\omega)}{1 + S_{\mathrm{e}}\sigma_z g_{00} - S_{\mathrm{m}}^2 p_F^2\,\bar{g}_0(\omega)\,g_0(\omega)}g_0(\omega)\right]\right\} \tag{A16}$$

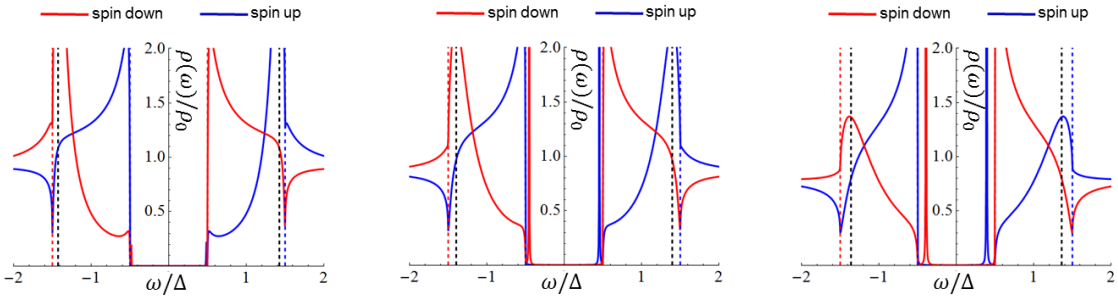

FIG. 5. (Color online) Spin-polarized local density of states (SP-LDOS) at the core of the skyrmion. The consequent panels correspond to increasing skyrmion size (a) $R = 1.1p_F^{-1}$, (b) $R = 1.2p_F^{-1}$, (c) $R = 1.3p_F^{-1}$. Other parameters are the same as in Fig. 2.

Appendix B: Wave function of the resonance

In this section, we discuss the wavefunction corresponding to SYSR resonance. The treatment is analogous to the discussion of T-matrix in the previous setion. We write Eq. (A1) in the form of the BdG equation in the momentum space

$$[\omega - h(\boldsymbol{p})]\,\Psi(\boldsymbol{p}) = \int \frac{d^2p'}{(2\pi)^2}\, V(\boldsymbol{p}-\boldsymbol{p}')\,\Psi(\boldsymbol{p}'), \qquad \text{(B1)}$$

where $\Psi(\boldsymbol{p})$ is the four-component wave function in the $\sigma\otimes\tau$ space. We substitute Eq. (A7) in the right hand side of Eq.(B1), use the definition of Green's function (A9) and obtain

$$\Psi(\boldsymbol{p}) = -g(\boldsymbol{p})\left(S_{\rm e}\sigma_z + iS_{\rm m}\boldsymbol{\sigma}\cdot\boldsymbol{p}\right)\,\Phi_1 - i\,g(\boldsymbol{p})S_m\sum_{j=x,y}\sigma_j\Phi_{2j}, \qquad \text{(B2)}$$

where Φ_1 and Φ_{2j} are the unknown four-component spinors defined self-consistently via wave function as

$$\Phi_1 = \int \frac{d^2p'}{(2\pi)^2}\,\Psi(\boldsymbol{p}'), \quad \Phi_{2j} = \int \frac{d^2p'}{(2\pi)^2}\,p'_j\Psi(\boldsymbol{p}'). \qquad \text{(B3)}$$

Therefore, we close the equations by substituting (B2) in Eq. (B3), take the integrals and obtain the following equations for the spinors

$$\Phi_1 = -S_{\rm e}g_0\sigma_z\Phi_1 - iS_{\rm m}g_0\sum_{j=x,y}\sigma_j\Phi_{2j}, \qquad \text{(B4)}$$

$$\Phi_{2j} = \frac{i}{2}S_{\rm m}p_F^2 g_0\sigma_j\Phi_1. \qquad \text{(B5)}$$

We substitute Eq. (B5) in Eq. (B4) and obtain the equation for Φ_1

$$\left[1 + S_{\rm e}g_0\sigma_z\,\Phi_1 - S_{\rm m}^2p_F^2\,g_0\bar{g}_0\right]\Psi_1 = 0. \qquad \text{(B6)}$$

This derivation is equivalent to the T-matrix treatment, and, therefore, notice that Eq. (B6) corresponds to finding kernel of the denominator of T-matrix (A11). Since the matrix expression in the square brackets contains only σ_z and τ_x matrices, the spinor Ψ_1 is an eigenstate of these matrices defined as $\tau_x\,|\pm\rangle = \pm\,|\pm\rangle$ and $\sigma_z\,|\uparrow\downarrow\rangle = \pm\,|\uparrow\downarrow\rangle$. That is the spinor for the positive SYSR state is $\Phi_1 = |\uparrow\rangle\otimes|+\rangle$ and negative - $\Phi_1 = |\downarrow\rangle\otimes|-\rangle$, just as for the usual YSR state. We also substiute Eq. (B5) in Eq. (B2) and obtain

$$\begin{aligned}\Psi(\boldsymbol{p}) &= -g(\boldsymbol{p})\left(S_{\rm e}\sigma_z + iS_{\rm m}\boldsymbol{\sigma}\cdot\boldsymbol{p} - S_{\rm m}^2p_F^2\bar{g}_0\right)\Phi_1,\\ &= -g(\boldsymbol{p})\left(S_{\rm e}\sigma_z - S_{\rm m}^2p_F^2\bar{g}_0\right)\Phi_1 - iS_{\rm m}g(\boldsymbol{p})\,\boldsymbol{\sigma}\cdot\boldsymbol{p}\,\Phi_1.\end{aligned} \qquad \text{(B7)}$$

In order to find the wave function in the real space one has to Fourier transform Eq. (B7). It can be done carefully but the resulting equations are bulky and obscure, so we are just going to show that the first term in the second line of Eq. (B7) gives exponentially localized wavefucntion, whereas the last term has a powerlaw decay and is thus long-ranged. The key element is finding the Fourier transform of the Green's function which we expand using the projector operators $(1\pm\sigma_z)/2$

$$\begin{aligned}g_{\boldsymbol{r}} &= \int\frac{d^2p}{(2\pi)^2}g(\boldsymbol{p}) = \sum_{\lambda=\pm}\frac{1+\lambda\sigma_z}{2}\,g^\lambda_{\boldsymbol{r}}, \quad \text{where}\\ g^\lambda_{\boldsymbol{r}} &= \int\frac{d^2p}{(2\pi)^2}\frac{e^{i\boldsymbol{p}\boldsymbol{r}}}{\omega_\lambda - \xi\tau_z - \Delta\tau_x},\ \omega_\lambda = \omega - \lambda S.\end{aligned} \qquad \text{(B8)}$$

The integral in Eq. (B8) can be evaluated for $r \gg v_F/\omega_D$ [31], where ω_D is the Debye energy,

$$\begin{aligned}g^\lambda_{\boldsymbol{r}} &= -\pi\rho\left\{\frac{(\omega_\lambda + \Delta\tau_x)}{2\sqrt{\Delta^2-\omega_\lambda^2}}\left[f_1(\boldsymbol{r}) + f_2(\boldsymbol{r})\right] + \tau_x\left[f_1(\boldsymbol{r}) - f_2(\boldsymbol{r})\right]\right\},\\ \text{where}\ \ f_1(\boldsymbol{r}) &= J_0\left[(p_F + ip_\lambda)\,r\right] + H_0\left[(p_F + ip_\lambda)\,r\right],\\ f_2(\boldsymbol{r}) &= J_0\left[(p_F - ip_\lambda)\,r\right] - H_0\left[(p_F - ip_\lambda)\,r\right],\\ p_\lambda &= \frac{\sqrt{\Delta^2-\omega_\lambda^2}}{v_F},\end{aligned} \qquad \text{(B9)}$$

where J_0 and H_0 are the Bessel and Struve functions, p_F - Fermi momentum, p_λ characteristic momentum of

a superconductor. Although the Green's function in the real space is quite bulky, it has a simple assymptotic behavior at $r \gg \xi_{sc}$

$$g^{\lambda}_{\boldsymbol{r}} \sim \frac{e^{ip_F r} e^{-p_\lambda r}}{\sqrt{r}}. \tag{B10}$$

The first term describes fast Friedel oscillations, whereas second term - behavior at a scale of the superconducting coherence length ξ_{sc}. For the state inside the superconducting gap, i.e. for $|\omega_\lambda| < \Delta$, the latter term the exponential decay. In contrast for the state inside the continuum, i.e. for $|\omega_\lambda| > \Delta$, p_λ becomes imaginary, i.e. $p_\lambda = -i\sqrt{\omega_\lambda^2 - \Delta^2}/v_F$, and therefore the last exponential term in Eq. (B10) describes periodic oscillations with a period $\Delta r \sim 1/\xi_{sc}$.

The polarized SYSR state discussed above lies inside the continuum of states corresponding to the opposite spin polarization. Moreover, the last term in Eq. (B7) describes the coupling of the state to the continuum of the background delocalized states. Thus, the SYSR is expected to have an oscillating power-law rather than decaying behavior as also supported by the numerics.